Strong surface winds in Storm Eunice. Part 2: airstream analysis

Volonté, A. ORCID: https://orcid.org/0000-0003-0278-952X, Gray, S. L. ORCID: https://orcid.org/0000-0001-8658-362X, Clark, P. A. ORCID: https://orcid.org/0000-0003-1001-9226, Martínez-Alvarado, O. ORCID: https://orcid.org/0000-0002-5285-0379 and Ackerley, D. (2024) Strong surface winds in Storm Eunice. Part 2: airstream analysis. Weather, 79 (2). pp. 54-59. ISSN 1477-8696 doi: 10.1002/wea.4401 Available at https://centaur.reading.ac.uk/111439/

Strong surface winds in Storm *Eunice*. Part 2: airstream analysis

Ambrogio Volonté[1,*], Suzanne L. Gray[1], Peter A. Clark[1], Oscar Martínez-Alvarado[1,2] and Duncan Ackerley[3]

[1]*Department of Meteorology, University of Reading, UK*
[2]*National Centre for Atmospheric Science, University of Reading, UK*
[3]*Met Office, Exeter, UK*

Introduction

Strong, damaging winds over widespread areas, or windstorms, are generally associated with cyclones. Research has shown that the highly asymmetric nature of extratropical cyclones leads to strong winds in different regions of a storm and at different stages in the storm's lifecycle. This presents an additional forecasting challenge. Not only do we need to predict the path and overall strength of a storm, but also when and hence where, geographically, these different regions within the storm might occur.

Three of the strong wind regions were identified many decades ago as the structure of extratropical cyclones was elucidated (Dacre, 2020). The 'warm conveyor belt' (WCB; Browning, 1971) starts in the warm-sector boundary layer as a jet associated with the trailing cold front before rising above the warm front. The 'cold conveyor belt' (CCB), on the cold side of the occluded or 'bent-back' front, wraps cyclonically around the cyclone centre at low levels (Schultz, 2001) and often produces strong winds only once it turns broadly into the direction that the cyclone is moving. Strong winds associated with the upper-level jet descend towards the cyclone centre as a 'dry intrusion' (DI) and can, sometimes, contribute to surface winds and gusts, often via deep convection (Browning and Roberts, 1994; Raveh-Rubin, 2017). The DI can also overrun the surface cold front leading to a 'shallow moist zone' and upper-level front (mainly due to a humidity contrast) ahead of the surface cold front (see fig. 11 in Browning and Roberts, 1994). A fourth region, called the 'sting jet' (SJ), was first proposed by Browning (2004) from analysis of the 'Great Storm' of 1987. The SJ occurs in the 'frontal-fracture' region of storms with a particular structure; these storms follow the Shapiro–Keyser cyclone model (Shapiro and Keyser, 1990). SJs descend from the storm 'cloud head' and, if they reach the surface at all, do so ahead of the CCB for only a few hours. SJs are especially difficult to detect unequivocally in observations, and much of our understanding of them stems from model simulations with sufficiently high resolution to represent them. The first example of SJ identification in model simulations, again in the 1987 'Great Storm', was reported by Clark *et al*. (2005) and shows a narrow (~50km) jet descending from mid-levels in the storm's 'cloud head' to the surface. In the case of the 'Great Storm', the SJ was responsible for most of the storm damage.

Storm *Eunice* was the second of three named storms to affect the United Kingdom (UK) within a week during February 2022 and, although not as devastating as the Great Storm (not least because of the actions taken as a result of the warning), *Eunice* produced record-breaking wind gusts over England and led to severe weather impacts in the UK and Ireland including fatalities, power and transport disruption, thousands of felled trees, and the closure of schools and businesses. An account of the impacts and observations for all three named storms, together with the historical context of Storm *Eunice*, is given in a Met Office report (Kendon, 2022).

The companion article containing the first of this two-part study (Volonté *et al*., 2023) shows how *Eunice* displayed, in observations and model forecasts, several specific features indicating the likely presence of SJ activity, such as its Shapiro–Keyser structure and the evident banding at the tip of the bent-back cloud head present for several hours in satellite imagery. *Eunice* was forecast to become an intense cyclone several days in advance of its occurrence and the SJ precursor diagnostic tool, described in Gray *et al*. (2021) and available to Met Office operational forecasters, provided further indications of the potential for SJ activity up to three days in advance. However, uncertainty on the exact location and strength of near-surface peak winds was present in operational Met Office model forecasts even at lead times of a few hours. These results provide a strong indication that SJ activity is likely to have occurred, and lasted for an extended period of time, during the evolution of Storm *Eunice*. However, they are not sufficient to assess whether the strong surface winds and gusts observed over South England and Wales in the central hours of 18 February were associated solely with the descent of a SJ or whether additional, or different, airstreams were involved. For this reason, and to provide more certainty on the identification of SJ activity, a detailed analysis of the main low-level airstreams present in Storm *Eunice* and of the underlying cloud head dynamics was performed using Met Office operational model data and is presented in this article. This analysis takes advantage of both Eulerian and Lagrangian perspectives, using an extensively tested methodology, previously applied to several other cases of UK SJ cyclones (see Clark *et al*., 2005; Martínez-Alvarado *et al*., 2014; Volonté *et al*., 2018, among others). The following two key questions are answered:

1. *Sting jet presence*: Was SJ activity present in Storm *Eunice* and, if so, at what point and for how long in the storm's lifecycle did the SJ activity take place?
2. *Cause of peak surface winds and gusts*: Which of the strong wind regions expected in a storm such as *Eunice*, including any possible SJs, led to the observed near-surface peak winds and gusts (that occurred over southeast England at about 1200 UTC on 18 February)?

Analysis of airstreams associated with strong surface winds: Eulerian analysis

The first part of this airstream analysis is conducted with an Eulerian approach, that is, assessing the motion of the airstreams from specific locations, rather than following the air parcels with time.

Potential vorticity evolution

As previously explained in the part 1 article of this study, the slantwise circulations associated with SJ descent, of which the cloud head banding is interpreted as evidence, can be caused by the release of mesoscale instabilities such as conditional symmetric instability (CSI). Symmetric instability (SI), the dry counterpart of CSI, is more immediately related to slantwise motions, as air saturation is not needed for its release. However, SI is also defined by stricter conditions and, while the presence of SI implies the presence of CSI, the opposite is

not true and not all regions with CSI will also have SI. Recent work on idealised SJ cyclones (Volonté *et al.*, 2020) has shown that in intense Shapiro–Keyser cyclones it is not uncommon that even SI is generated in the cloud head and then released during SJ descent. SI is indicated by negative values of potential vorticity (PV). Forecast PV on a 700hPa surface between 2100 UTC on 17 February and 0300 UTC on 18 February in the Met Office global model is shown in Figure 1. This part of the evolution of Storm *Eunice* is selected because of the clear banding at the tip of the cloud head at these times (see figs. 3b and c and related discussion in the part 1 article). Figure 1 also illustrates the mid-tropospheric structure of *Eunice* with contours of wet-bulb potential temperature, θ_w, indicating the location of warm and cold sectors and fronts, together with black dashed contours enclosing the areas where clouds are present (both fields are also shown at 700hPa).

Elongated structures of negative PV, indicating the presence of SI, develop in the late hours of 17 February on the cold side of the warm front, highlighted by the sharp gradient in θ_w contours north of the cyclone centre (where PV instead has high values, well above zero). These features move rearwards with respect to the centre of the storm, towards the tip of the cloud head as it develops and starts bending back (Figures 1a and b). By the early hours of 18 February, those features move towards the cloud head tip, which at the same time starts wrapping around the cyclone centre and consequent warm seclusion (Figure 1c). The front edge of this negative PV region is collocated with a gap or hole that develops in the cloud (Figure 1d, see the black arrow). This cloud break is consistent with the banding observed in satellite imagery at relevant times (see figs. 3b and c in the part 1 article), indicating that the feature is likely to be realistic, rather than a model artefact. The flow in this region is descending (as it is shown later on in this analysis) and this cloud gap can thus be related to the evaporation occurring during the slantwise descent of air parcels associated with negative PV (i.e. SI).

In summary, the evolution of PV in the cloud head in the form of elongated bands of symmetrically unstable air travelling towards the cloud head tip and associated with a descending, drying airstream, as confirmed by satellite observations is consistent with SJ development.

Three-dimensional structure of low-level jets

Considering horizontal maps and vertical cross-sections from the global model shown in Figure 2, we now identify the various low-level wind maxima present at different stages in the evolution of Storm *Eunice*, describing their 3-dimensional structures.

At 0100 UTC on 18 February, the cyclone was still over the Atlantic and the strongest winds over southern England would only be recorded ≈10h later. However, as mentioned earlier, at this stage the cloud head was well formed and banding was present at its tip. Figure 2(a) shows two wind speed maxima exceeding 44ms^{-1} at the pressure level of 850hPa, either side of the warm seclusion at the cyclone centre, indicated by the higher θ_w values.

The associated vertical cross-section (Figure 2b) shows that the western maximum, with θ_w between 276 and 278K, is in cloud and centred at ~900hPa, with peak speed above 46ms^{-1} and the 30ms^{-1} envelope extending down to the surface. This wind maximum is located on the cold side of the bent-back front, indicated by the tight gradient in θ_w. These features are typical of the CCB airstream, travelling at low levels in the cloud head while gradually wrapping around the cyclone centre.

The eastern wind maximum is mostly cloud-free and not on the cold side of the bent-back front. Its θ_w, between 278 and 279K, is characteristic of the cold frontal surface but it is not associated with a strong horizontal gradient in θ_w, though by this time the warm seclusion has formed and forms the western boundary of the maximum; it is located just beyond the cloud-head tip and thus at the entrance of the developing frontal-fracture region, indicated by the increasing gap between θ_w contours. These features are all consistent with the wind maximum being part of a SJ, although contribution from the leading edge of the CCB cannot be excluded without further evidence.

At the same time, it should be noted that strong winds associated with the upper-level jet and the related tropopause fold extend all the way down to the lower troposphere (see the 50ms^{-1} wind speed contour down to ~700hPa). A similar feature is seen in fig. 4 of Volonté *et al.* (2018), although at higher levels (around 600hPa). This downward, slanted, protrusion of strong winds is aligned with the cold front and associated with a notch of dry air in the warm-sector cloud, suggesting it is linked to the DI overrunning the surface cold front.

A relatively weak wind maximum (the 30ms^{-1} wind speed contour) is seen at about 900–950hPa to the east of the cold front, with $\theta_w \sim 285$K. Being in the warm sector and in cloud, this wind feature could be part of the WCB, although the likely presence of vertical motion at the nearby cold front transporting slower air upwards (see ridge in the green contour) and the close presence of DI air complicate the picture

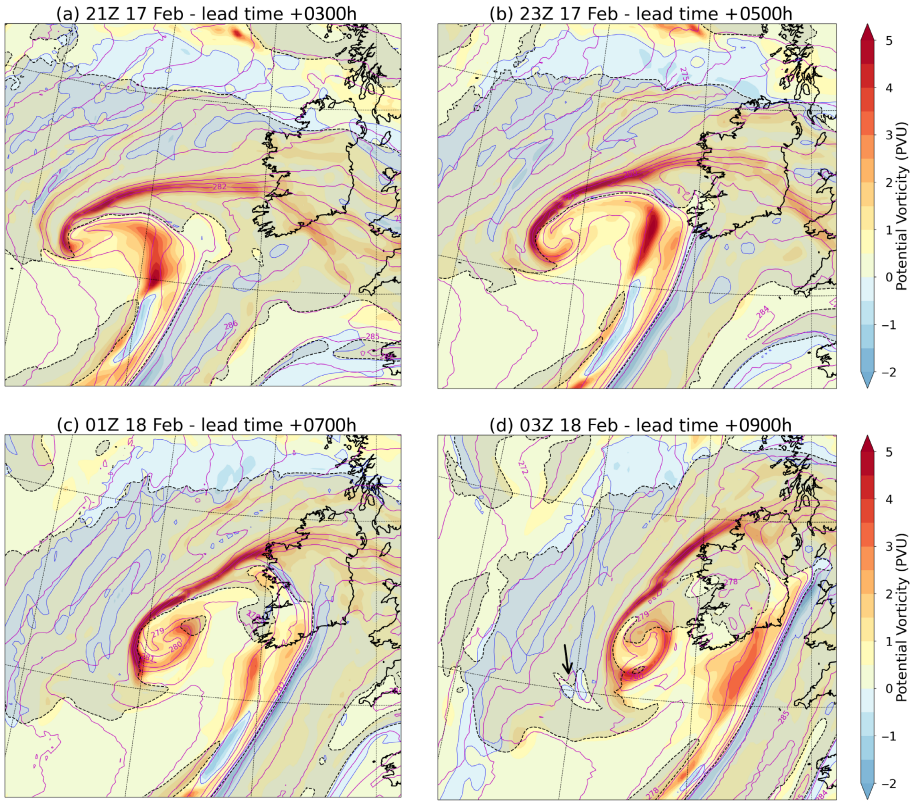

Figure 1. Potential vorticity (shading, PVU), wet-bulb potential temperature (magenta contours, every 1K) and relative humidity with respect to ice (dashed black contours, 80%, and semi-transparent grey shading, 80% and above) from Met Office global operational forecasts initialised at 1800 UTC on 17 February (valid and lead times indicated on top of each panel). All quantities are displayed at 700hPa. The black arrow in panel (d) indicates the location of the cloud hole described in the text.

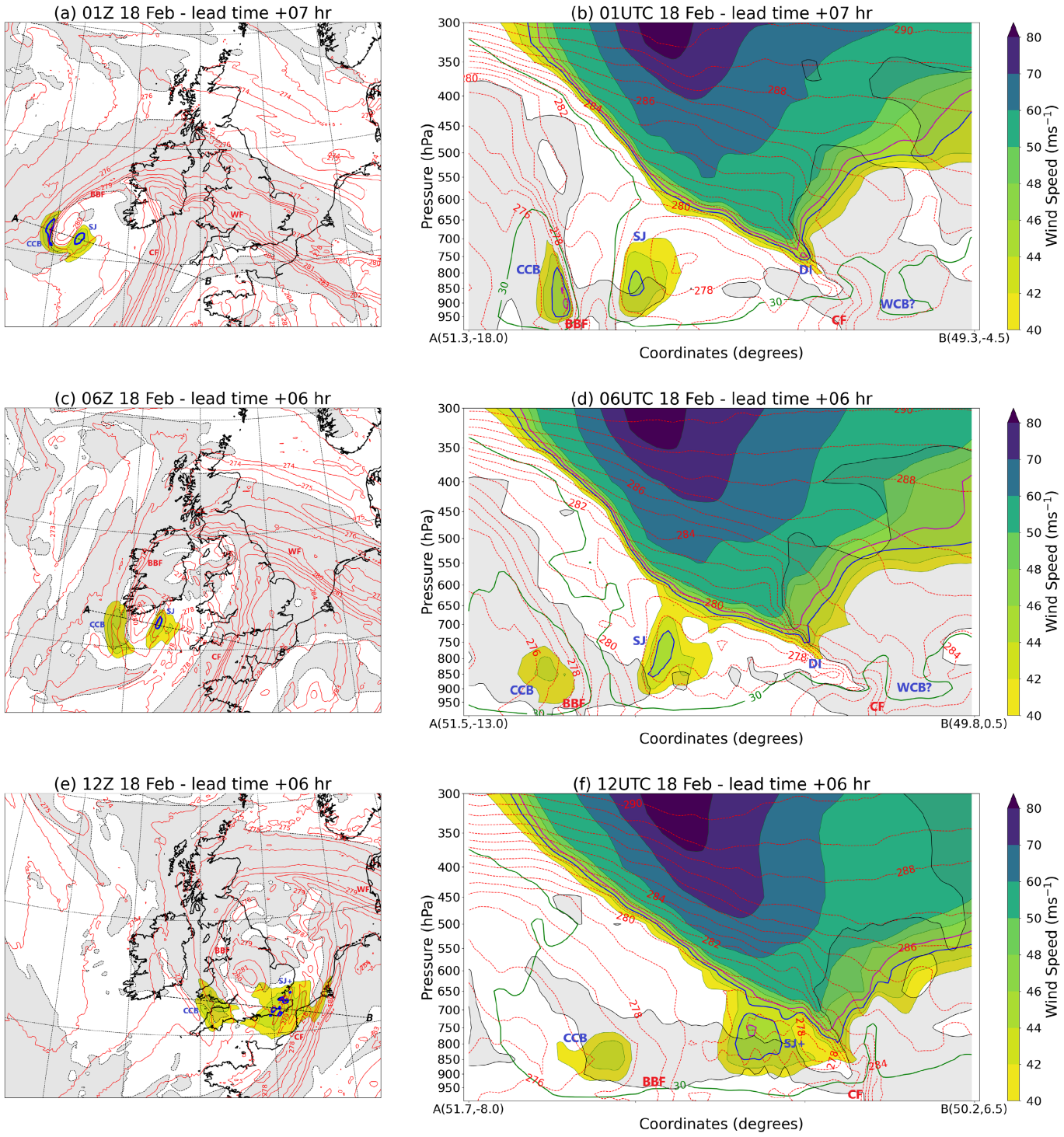

Figure 2. (a, c, e) Horizontal wind speed at 850hPa (ms^{-1}, shading with non-uniformly spaced scale, and 44 and 46ms^{-1} contours highlighted in blue and magenta, respectively), wet-bulb potential temperature at 850hPa (red contours, every 1K) and relative humidity with respect to ice at 700hPa (grey shading, >80%). (b, d, f) Vertical cross-sections of the same quantities, plus 30ms^{-1} wind speed contour (green line), evaluated on transect AB in maps (a, c, e). The airstreams discussed in the text are annotated in blue in all panels, while frontal features (cold front [CF], warm front [WF], bent-back front [BBF]) are annotated in red. Data from Met Office global operational forecasts initialised at (a, b) 1800 UTC on 17 February, (c, d) 0000 UTC on 17 February, (e, f) 0600 UTC on 18 February (valid and lead times indicated on top of each panel).

(and the feature is therefore indicated with 'WCB?' in the vertical cross-sections).

Both wind speed maxima, eastward and westward of the cyclone centre (associated respectively with SJ and CCB), are still present at 0600 UTC (Figures 2c and d). While the SJ maximum winds retain a similar intensity to the previous stage, the CCB wind peak is now ~4ms^{-1} weaker and more extended horizontally. Contextually, the bent-back front is now more slanted and less sharp than earlier on. The SJ maximum is now more elongated into the frontal-fracture region, and the vertical cross-section shows that it lies at the bottom of an area of descending and buckling moist isentropes (θ_w contours). This is further indication of the descent of a coherent airflow, reinforcing the hypothesis that this wind maximum is associated with a SJ (θ_w is conserved along the flow of a distinct air parcel that does not experience substantial radiative heating or cooling or turbulent mixing and thus we can assume that such an airflow will move along moist isentropes).

At 1200 UTC the cyclone is in its mature stage, with strong near-surface winds

affecting southern England. This is shown in Figures 2(e) and (f), with the western wind maximum (CCB) now located over the Bristol Channel and the eastern maximum (SJ), more intense, centred over the southeast corner of England. As the weakening of the bent-back front continues and the frontal-fracture region begins to close, the separation between air masses in the cold sector, frontal-fracture region and warm sector becomes less clear. As a result, the lower edge of the 30ms^{-1} envelope is now down to near-surface heights across most of the region covered by Figure 2(f). By this time, the wind maximum in the frontal-fracture region is closer to the primary cold front and mixing of SJ air with the dry-air notch near the front cannot be excluded. Wind speed values peak above 46ms^{-1} at around 750hPa and exceed 44ms^{-1} down to 850hPa, at the top of the boundary layer where oscillations in cloud base height and θ_w contours indicate the presence of convective and/or turbulent motions. These features, if real and not just an artefact of the model struggling to simulate a strongly vertically sheared top of the boundary layer with low static stability, could have played a role in aiding the downward transfer of momentum towards the surface and the formation of local peak gusts. This would be consistent with the dynamics shown by previous case-study (Browning *et al*., 2015) and idealised (Rivière *et al*., 2020) research. Along the cold front, the bottom edge of the strong winds associated with the DI comes closer to the frontal-fracture region wind maximum, suggesting possible influence on it. Strong winds associated with the WCB are also located close to this wind maximum, albeit on the other side of the sloping cold front (see rightmost dip in the 40ms^{-1} filled contour). Therefore, while its location in the frontal-fracture region and at the end of downward sloping θ_w contours still indicates that the frontal-fracture wind maximum is associated with SJ descent, contributions from multiple other airstreams are likely (and for this reason we indicate it with 'SJ+' in Figures 2(e) and (f)).

In summary, analysis of horizontal and vertical slices through the model output strongly suggests that the two regions of strong surface winds present in the early hours of 18 February are due to separate jets: the CCB jet to the west and SJ to the east. By 1200 UTC, the lower edge of the upper-level jet is down to the mid-troposphere (as indicated by the 70ms^{-1} contour near 500hPa) and the tropopause fold has descended into the lower troposphere. At this time, the eastern region of strong winds is located just behind the cold front and near the fold, making the interpretation of the cause of the strong winds more difficult. Lagrangian trajectory analysis, as described next, can be used to unpick the different contributions to the strong wind regions.

Analysis of airstreams associated with strong surface winds: Lagrangian analysis

The second part of this airstream analysis is conducted with the alternative Lagrangian trajectory approach, that is, following the air parcels with time rather than assessing the motion of the airstreams from specific locations, to identify the characteristics of air flows associated with the different jets within cyclones.

Using the wind field components at each grid point 'parcels' of air are traced forwards and/or backwards in time to produce trajectories. Clusters, sometimes called 'coherent ensembles', of trajectories define the jets. Although trajectories can be produced starting from any model grid point, typically these 'start points' of the trajectories are restricted geographically and by thresholds on fields such as wind speed (e.g. restricted to specific strong wind regions within the weather system). The model output used must extend over the time period that trajectories are calculated and more accurate trajectories are generated with more frequent output.

Here the trajectory calculation code LAGRANTO (Sprenger and Wernli, 2015) has been used to calculate trajectories using hourly global Met Office model forecast output. Figure 3 shows trajectories with start points (black dots) in the strong low-level wind regions at 1200 UTC 18 February, when the strongest winds crossed over southeast England (including London). A wind speed threshold of 42ms^{-1} is used to select the cores of the air flows (a balance between having so many trajectories that they are difficult to interpret and so few so that they are not representative). The trajectories are coloured by air pressure so that descending air is shown by a change from cooler to warmer colours, and air moves along all the trajectories with an eastwards component. The start points in Figure 3(a) are clustered into two sets, over south Wales/the Cornish Peninsula and southeast England, consistent with the wind speed map shown in Figure 2(e). The associated sets of trajectories form two broad overlapping clusters, crossing southwards over Ireland towards the more westward start points and originating further south with a northward component on approaching the more eastwards start points. The air generally descends as it moves towards the start points.

More information about air flows is obtained by adding additional selection criteria as in Figures 3(b–d). For these panels, the possible start point locations have been extended slightly in the vertical compared with Figure 3(a) so that jets that lead to strong low-level winds, but are centred above this level (i.e. only the lower part of the jet reaches low levels), are captured. Comparison of Figure 3(a) with Figures 3(b–

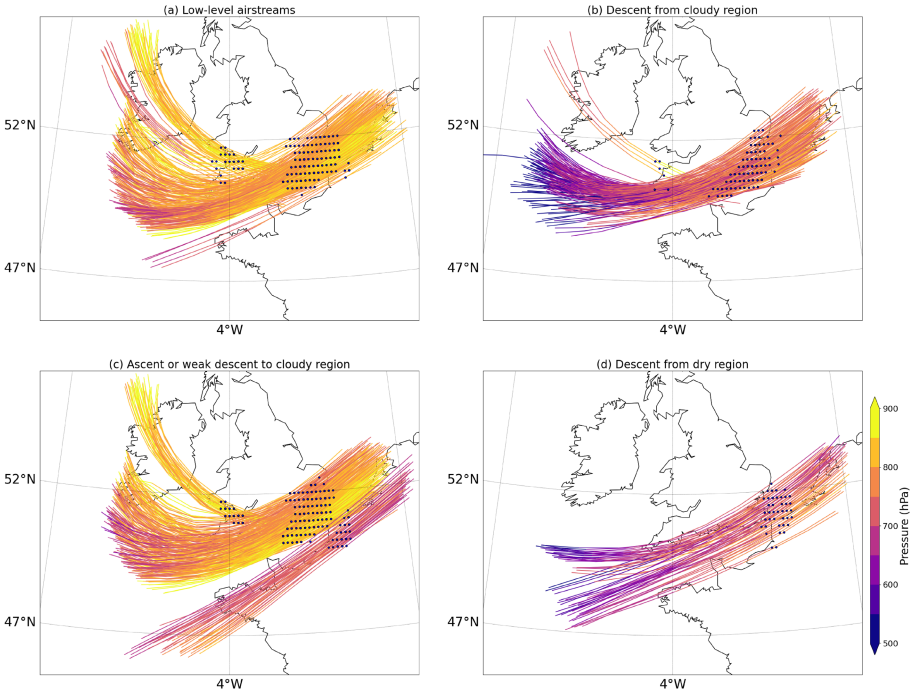

Figure 3. Lagrangian trajectories starting at 1200 UTC on 18 February (forecast start time 0600 UTC), running backward for six hours and forward for two hours and shaded by air pressure. Starting points are defined by wind speed >42ms^{-1} and pressure between 950 and 800hPa for panel (a) and between 950 and 700hPa for other panels. Horizontal starting domain is 4°W–3°E and 50–53°N for all panels. Additional conditions (listed in the text) applied in panels (b–d) to isolate and characterise the airstreams are summarised in the panel titles.

d) shows that all the jets leading to strong near-surface winds are captured by the additional selection criteria; these jets are shown schematically in Figure 4 (which presents a synthesis of the jets in Storm *Eunice*). Figure 3(b) shows trajectories that originate in cloudy air (defined as relative humidity with respect to ice >80%) and descend at least 100hPa in the six hours before the time of the trajectory start points at 1200 UTC. These criteria identify the SJ descending from the cloud head tip towards the top of the atmospheric boundary layer. Note that these SJ trajectories dry during descent (not shown), although trajectories forming the lower part of the jet later re-moisten as they intersect the boundary layer.

Figure 3(c) shows trajectories that either weakly descend or ascend (descent <100 hPa) in the six hours before 1200 UTC and are in cloudy air at 1200 UTC. Three clusters of trajectories are identified. Analysis of the θ_w values of the three trajectory clusters (not shown) shows that each cluster has a distinct set of values at the time of the start points and thus is associated with a distinct region of Storm *Eunice*. The first cluster of trajectories, associated with start points over south Wales/the Cornish Peninsula, is the coldest and forms the CCB jet. The air in this jet wraps around the cyclone to the cold side of the bent-back front. The second cluster of trajectories, associated with start points over southeast England, has temperatures between those of the WCB and CCB jet. The majority of these trajectories are cloudy at 0600 UTC as well as at 1200 UTC and these trajectories start in the lower, cloudy part of the more eastwards strong wind region in Figure 2(f), where weak θ_w gradients indicate frontal fracture. These trajectories have a mix of characteristics. Some form the lower, more weakly descending portions of the SJ or DI, which become cloudy as they interact with the boundary layer air, whereas others may be SJ trajectories that have descended at an earlier time before spreading out within the SJ region or an earlier (warmer) branch of CCB jet air that has moved around the low centre to undercut the SJ; this jet is labelled as 'possible CCB2' in Figure 4. This mix of characteristics is quite typical in the mature frontal-fracture region where the SJ, having spread horizontally ahead of the CCB, becomes hard to distinguish from it. The third cluster of trajectories, associated with start points over the region of the France/Belgium border, has relatively low pressures and so the trajectories are higher in altitude than the other trajectories. They are also the warmest and are mostly cloudy along the entire trajectory (not shown); comparison of the start point locations with θ_w contours in Figure 2(e) shows that these trajectories are embedded in the cold frontal region and likely form an upper part of the WCB jet. Although these trajectories do not descend to the surface, line convection (visible on radar imagery, not shown) in this region may have brought some high momentum air down to the surface so contributing to strong winds.

Finally, Figure 3(d) shows trajectories that descend at least 100hPa in the six hours before 1200 UTC and originate in dry air (defined as relative humidity with respect to ice <60%). The associated start points lie above (have lower pressures) and are slightly ahead (to the east) of the southeast England start points shown in Figure 3(c), extending offshore and over the near continent. These criteria identify the DI, which can also be seen as strong winds extending down to low levels on the right-hand side of Figure 2(f).

Trajectories have also been calculated that have their start points in the low-level strong wind regions at 0100 and 0600 UTC on 18 February (using the slightly weaker wind threshold of 40ms^{-1}, not shown). At these earlier times, there is little evidence of a DI jet (just a few trajectories meet the above criteria at 0600 UTC) as it has not descended as far (compare Figures 2b, d and f). However, trajectories meeting the criteria above for a SJ and CCB jet exist at both times. In summary, the Lagrangian trajectory analysis reveals that, while distinct strong wind regions attributable to the CCB jet and SJ exist at earlier times, the strong winds over southeast England at 1200 UTC on 18 February cannot be attributed to a single jet. Instead, there are contributions from a SJ, the DI and possibly also an earlier branch of the CCB jet (CCB2).

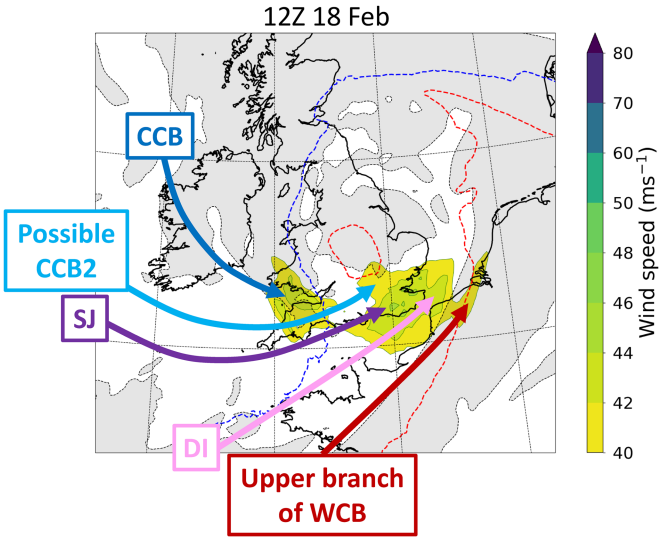

Figure 4. Schematic, adapted from Figure 2(e), illustrating the airstreams associated with strong winds over southeast England and nearby regions at 1200 UTC on 18 February. The schematic includes horizontal wind speed at 850hPa (shading, ms^{-1}), θ_w at 850hPa (dashed contours, red for 280K and blue for 277K), and relative humidity with respect to ice at 700hPa (grey shading, >80%).

Conclusions

Storm *Eunice* was an intense windstorm that affected the UK on 18 February 2022, triggering the first Met Office red warning for wind over southeast England since the National Severe Weather Warning Service was set up in the wake of the Great Storm of 1987. As shown in the first article of this two-part study (Volonté *et al.*, 2023), Storm *Eunice* produced record-breaking wind gusts and led to severe weather impacts, including fatalities. Weather station observations and satellite imagery provided strong indications of the likelihood of SJ activity taking place, as also did the SJ precursor diagnostic tool, described in Gray *et al.* (2021) and available to Met Office operational forecasters, up to three days in advance. While *Eunice* was forecast to become an intense cyclone several days in advance, uncertainty on the exact location and strength of near-surface peak winds remained in operational Met Office model forecasts up to a few hours before its passage.

Starting from these indications, the detailed analysis of the main low-level airstreams present in Storm *Eunice* and of the underlying cloud-head dynamics fully addresses the key questions (listed in the Introduction section) on the presence and longevity of a SJ and on the identification of the airstream(s) associated with the peak winds and gusts over southeast England.

Met Office operational short-lead-time forecasts highlight the development of narrow elongated regions of negative PV in the cloud head at mid-levels at the time of opening of the frontal fracture. These filaments, indicating the presence of a type of mesoscale instability (SI) in the cloud head, travel towards the tip of the cloud head at the end of the bent-back front, and one of them is associated with a hole opening up in the cloud. This evolution is consistent with satellite imagery and is a typical sign of SJ development in the cloud head. Focusing on the 3-dimensional structure of wind maxima in the lower troposphere, two wind maxima are present over an extended

time period during Storm *Eunice*'s lifecycle. Both wind maxima, located either side of the warm seclusion denoting the centre of the storm, exceed 46ms^{-1} at times. The western maximum is associated with air travelling at low levels in a stable boundary layer on the cold side of the bent-back front, while the eastern maximum is associated with air with intermediate θ_w values descending into the cloud-free frontal-fracture region. Therefore, we concluded that these two wind maxima are caused by CCB and SJ airstreams, respectively. By the time Storm *Eunice* reaches Wales and southern England, the cyclone is entering its mature stage with the frontal-fracture region beginning to close and becoming less clearly separated from air masses in the cold and warm sectors of the storm. As the tropopause fold continues to extend downward, DI air also reaches low levels. In this situation, Lagrangian air parcel trajectories are needed to separate the individual airstreams causing the large area of winds with speeds exceeding 40ms^{-1} approaching the lower troposphere. Back-trajectories starting from low-level strong wind regions (>42ms^{-1}) reveal that at 1200 UTC on 18 February, the time when strongest winds affected southeast England, the frontal-fracture region wind maximum contains descending air of mixed origin. The main airstreams associated with it are CCB and SJ, but there are contributions from the DI and even air parcels from the WCB are detected nearby.

In conclusion, the two key questions of this article (listed in the Introduction section) can be answered as follows:

1. *Sting jet presence*: SJ activity was detected over an extended time period during the evolution of Storm *Eunice*. There is evidence of cloud-head mesoscale instability presence and release, which will have enhanced the strength of the SJ. Descending SJ air was more clearly identifiable during the early hours of 18 February, when *Eunice* was still over the Atlantic Ocean and southwest of Ireland. However, SJ air was still present in the central hours of that day, when *Eunice* crossed southern England and Wales.
2. *Cause of peak surface winds and gusts*: The observed near-surface peak winds and gusts occurred in air associated with a mix of airstreams: the CCB and SJ, with a contribution from the DI (thanks to the particularly deep tropopause fold) and nearby presence of the WCB.

The complex mix of different airstreams leading to the strong winds observed over southern England and Wales in correspondence with the passage of Storm *Eunice* is synthesised, together with the individual airstream paths, by the schematic in Figure 4. A final remark on this analysis is that Storm *Eunice* showed that in strong SJ-capable extratropical cyclones, damaging winds can be caused by a number of different airstreams. While this inherent complexity adds to the beauty of such weather systems, it also implies that the understanding of the interaction between those airstreams and the forecasting of their, potentially very damaging, effects in terms of surface winds and gusts remain significant challenges.

Acknowledgements

The work performed by Ambrogio Volonté was funded by the 2022 pump-priming fund of the Department of Meteorology, University of Reading. Oscar Martínez-Alvarado's contribution was supported by the UK Natural Environment Research Council as a member of the National Centre for Atmospheric Science. Duncan Ackerley is supported by the Joint BEIS/Defra Met Office Hadley Centre Climate Programme (GA01101) and facilitated access to the relevant Met Office datasets. The authors would also like to thank Dan Suri for providing helpful insight to an earlier version of this work. No new datasets were created in this study. Operational forecast outputs used are archived at the Met Office; please contact the authors for details. Trajectory files can be provided upon request.

Author contributions

AV designed the study, retrieved model data and satellite imagery, and wrote a first draft of the article. SLG co-designed the study and provided maps of observed winds and gusts. PAC wrote the introduction of the article. OM-A analysed output from the precursor tool, provided by DA, and model forecasts. All authors took part in discussing the scope of the study and the results, and in revising the document through the peer-review process.

Data availability

No new data were created in this study.

References

Browning KA. 1971. Radar measurements of air motion near fronts. *Weather* **26**(8): 320–340.

Browning KA. 2004. The sting at the end of the tail: damaging winds associated with extratropical cyclones. *Q. J. R. Meteorol. Soc.* **130**: 375–399.

Browning KA, **Roberts NM**. 1994. Structure of a frontal cyclone. *Q. J. R. Meteorol. Soc.* **120**: 1535–1557.

Browning KA, **Smart DJ**, **Clark MR *et al***. 2015. The role of evaporating showers in the transfer of sting-jet momentum surface. *Q. J. R. Meteorol. Soc.* **141**(693): 2956–2971.

Clark PA, **Browning KA**, **Wang C**. 2005. The sting at the end of the tail: model diagnostics of fine-scale three-dimensional structure of the cloud head. *Q. J. R. Meteorol. Soc.* **131**: 2263–2292.

Dacre H. 2020. A review of extratropical cyclones: observations and conceptual models over the past 100 years. *Weather* **75**(1): 4–7.

Gray SL, **Martínez-Alvarado O**, **Ackerley D *et al***. 2021. Development of a prototype real-time sting-jet precursor tool for forecasters. *Weather* **76**(11): 369–373.

Kendon M. 2022. *Storms Dudley, Eunice and Franklin, February 2022*. Technical report. Met Office. https://www.metoffice.gov.uk/weather/learn-about/pastuk-weather-events. [accessed 10 March 2023].

Martínez-Alvarado O, **Baker LH**, **Gray SL *et al***. 2014. Distinguishing the cold conveyor belt and sting jet airstreams in an intense extratropical cyclone. *Mon. Weather Rev.* **142**: 2571–2595.

Raveh-Rubin S. 2017. Dry intrusions: Lagrangian climatology and dynamical impact on the planetary boundary layer. *J. Clim.* **30**(17): 6661–6682.

Rivière G, **Ricard D**, **Arbogast P**. 2020. The downward transport of momentum to the surface in idealized sting-jet cyclones. *Q. J. R. Meteorol. Soc.* **146**(729): 1801–1821.

Schultz DM. 2001. Reexamining the cold conveyor belt. *Mon. Weather Rev.* **129**(9): 2205–2225.

Shapiro MA, **Keyser D**. 1990. *Fronts, jet streams and the tropopause, in Extratropical cyclones: the Erik Palmén memorial volume*. Newton C, Holopainen EO (eds) . American Meteorological Society: Boston, MA, pp 167–191.

Sprenger M, **Wernli H**. 2015. The LAGRANTO Lagrangian analysis tool – version 2.0. *Geosci. Model Dev.* **8**: 2569–2586.

Volonté A, **Clark PA**, **Gray SL**. 2018. The role of mesoscale instabilities in the sting-jet dynamics of Windstorm Tini. *Q. J. R. Meteorol. Soc.* **144**: 877–899.

Volonté A, **Clark PA**, **Gray SL**. 2020. Idealised simulations of cyclones with robust symmetrically unstable sting jets. *Weather Clim.Dyn.* **1**(1): 63–91.

Volonté A, **Gray SL**, **Clark PA** *et al*. 2023. Strong surface winds in Storm *Eunice*. Part 1: storm overview and indications of sting-jet activity from observations and model data. Weather **78**: https://doi.org/10.1002/wea.4402

Correspondence to: A. Volonté
a.volonte@reading.ac.uk

doi: 10.1002/wea.4401